Chinese Journal of Catalysis 38 (2017) 918–927

available at www.sciencedirect.com

ScienceDirect

journal homepage: www.elsevier.com/locate/chnjc

Article

Investigation of low-temperature hydrothermal stability of Cu-SAPO-34 for selective catalytic reduction of NO_x with NH_3

Xiao Xiang [a,b], Pengfei Wu [a,b], Yi Cao [a], Lei Cao [a], Quanyi Wang [a], Shutao Xu [a], Peng Tian [a,#], Zhongmin Liu [a,*]

[a] *National Engineering Laboratory for Methanol to Olefins, Dalian National Laboratory for Clean Energy, Dalian Institute of Chemical Physics, Chinese Academy of Sciences, Dalian 116023, Liaoning, China*

[b] *University of Chinese Academy of Sciences, Beijing 100049, China*

ARTICLE INFO

Article history:
Received 5 March 2017
Accepted 9 April 2017
Published 5 May 2017

Keywords:
Cu-SAPO-34
Low temperature hydrothermal stability
Nitrogen oxides
Selective catalytic reduction
Ammonia oxidation

ABSTRACT

The low-temperature hydrothermal stabilities of Cu-SAPO-34 samples with various Si contents and Cu loadings were systematically investigated. The NH_3 oxidation activities and NH_3-selective catalytic reduction (SCR) activities (mainly the low-temperature activities) of all the Cu-SAPO-34 catalysts declined after low-temperature steam treatment (LTST). These results show that the texture and acid density of Cu-SAPO-34 can be better preserved by increasing the Cu loading, although the hydrolysis of Si–O–Al bonds is inevitable. The stability of Cu ions and the stability of the SAPO framework were positively correlated at relatively low Cu loadings. However, a high Cu loading (e.g., 3.67 wt%) resulted in a significant decrease in the number of isolated Cu ions. Aggregation of CuO particles also occurred during the LTST, which accounts for the decreasing NH_3 oxidation activities of the catalysts. Among the catalysts, Cu-SAPO-34 with a high Si content and medium Cu content (1.37 wt%) showed the lowest decrease in NH_3-SCR because its Cu^{2+} content was well retained and its acid density was well preserved.

1. Introduction

With the increasing number of diesel vehicles, nitrogen oxide (NO_x) emission control is becoming an important issue [1] because NO_x can lead to acid rain, photochemical smog, chronic damage to human health [2], and ground-level ozone generation. There is therefore an urgent need for the development of innovative post-combustion abatement systems. Among the available NO_x emission control techniques, selective catalytic reduction of NO_x with NH_3 (NH_3-SCR) is currently the most widely used method for NO_x reduction [3,4].

NH_3-SCR units are integrated with diesel particulate filters (DPFs) in emission control systems because of space limitations. Regeneration of the DPF needs high temperatures (>650 °C), therefore an NH_3-SCR catalyst needs to have excellent hydrothermal stability as well as high activity and selectivity over a wide temperature range. In recent decades, catalysts such as V-based oxides [5,6] metal-exchanged medium-pore zeolites [7,8], and Cu-exchanged small-pore zeolites [9,10] have been developed for NH_3-SCR processes. Currently, Cu-exchanged chabazites with eight-membered rings (e.g., Cu-SSZ-13 and Cu-SAPO-34) are among the most attractive NH_3-SCR catalysts.

* Corresponding author. Tel: +86-411-84379998; Fax: +86-411-84379289; E-mail: liuzm@dicp.ac.cn
# Corresponding author. Tel: +86-411-84379218; Fax: +86-411-84379289; E-mail: tianpeng@dicp.ac.cn

This work was supported by the National Natural Science Foundation of China (21676262, 21506207, 21606221) and the Key Research Program of Frontier Sciences, CAS (QYZDB-SSW-JSC040).
DOI: 10.1016/S1872-2067(17)62836-5 | http://www.sciencedirect.com/science/journal/18722067 | Chin. J. Catal., Vol. 38, No. 5, May 2017

These have been used in diesel emission control systems in the US and Europe. The superior high-temperature hydrothermal durabilities of Cu-SSZ-13 and Cu-SAPO-34 probably arise from the special topological structure and small pores of CHA [11]. Much research has focused on the catalytic properties of Cu-SSZ-13 catalysts, particularly the location and nature of the Cu species [12–14]. In contrast, Cu-SAPO-34 catalysts have been less investigated, although the high-temperature hydrothermal stability of Cu-SAPO-34 is better than that of Cu-SSZ-13 [11,15].

One disadvantage of SAPO-34 molecular sieves is their sensitivity to moisture below 100 °C, which is caused by hydrolysis of negative Si–O–Al bonds [16]. Previous studies have shown that the changes in the crystallinity and surface area of SAPO-34 arising from contact with room-temperature humidity for a short time are only partly reversible, and long-term contact of up to months or years can cause irreversible damage and even structural collapse [16]. The acid density of SAPO-34, which depends on its Si content and the Si environment, has an important effect on the sample's hydrothermal stability under ambient conditions: the higher the acid density, the lower the stability [16–18]. The low-temperature hydrothermal stability of Cu-exchanged SAPO-34, which is important for practical NH_3-SCR applications during engine cold starts, is not fully understood. Wang et al. [19] investigated the low-temperature stability of Cu-SAPO-34 synthesized using a one-pot method, with morpholine and a Cu–amine complex as templates, and showed that the introduction of Cu^{2+} enhanced the stability of SAPO-34. They found that samples with low Cu contents (0.35 and 1.70 wt%) had lower crystallinities, and fewer acid sites and isolated Cu species after exposure to humidity, resulting in a decrease in the low-temperature NH_3-SCR activity. Samples with high Cu contents (3.91 and 6.78 wt%) showed good retention of acid sites and isolated Cu species, and their low-temperature activities were therefore less affected. However, the distribution and proportion of Cu species in Cu-SAPO-34 synthesized using a one-pot method can differ from those in samples prepared using post-synthetic ion exchange. Leistner et al. [20] studied the low-temperature deactivation of Cu-SAPO-34 using elaborately designed experiments and observed severe loss of low-temperature NH_3-SCR activity after contact between the catalyst and water vapor at 70 °C for several hours. They found that the acidity and crystalline framework of SAPO-34 were little changed and attributed the activity loss to the transformation of active Cu species to inactive forms. Although useful information can be obtained from these studies, further research is needed because of the inconsistent conclusions. The evolution of Cu species on exposure to low-temperature moisture also needs to be further researched.

In the present work, two SAPO-34 supports with different Si contents (acid densities) were used to prepare Cu-SAPO-34 samples with various amounts of Cu to clarify the effects of low-temperature steam treatment (LTST) on the stability of Cu-SAPO-34. The effects of LTST of Cu-SAPO-34 on its Cu species and acid sites were investigated using N_2 physisorption, solid-state nuclear magnetic resonance spectroscopy (NMR), temperature-programmed desorption of NH_3 (NH_3-TPD), and electronic paramagnetic resonance (EPR) spectroscopy. The NH_3-SCR activities and NH_3 oxidation reactions over the Cu-SAPO-34 samples before and after LTST were examined and discussed in terms of the changes in the physicochemical properties of the catalysts.

2. Experimental

2.1. Catalyst preparation

SAPO-34 with a high Si content (denoted by H-Si) was synthesized from a gel of molar composition diethylamine/Al_2O_3/P_2O_5/SiO_2/H_2O = 2.0/1/1/0.8/50. Pseudo-boehmite (5.05 g, 72.5 wt%) was mixed with water (25.71 g) and then phosphoric acid (8.28 g, 85 wt%), silica sol (5.73 g, 30.1 wt%), and diethylamine (5.25 g) were sequentially added to the gel. The gel was transferred to a stainless-steel autoclave and crystallized at 200 °C for 48 h. The product was washed with deionized water and dried at 100 °C overnight.

SAPO-34 with a low Si content (denoted by L-Si) was synthesized from a gel of molar composition triethylamine/Al_2O_3/P_2O_5/SiO_2/H_2O = 3.0/1/1/0.2/50. The detailed synthetic procedure and crystallization conditions were similar to those used to prepare H-Si.

Cu-SAPO-34 was prepared using our recently reported direct ion-exchange (DIE) method [21]. This method simplifies the ion-exchange procedure and abates degradation of the SAPO framework during ion exchange. The synthesized SAPO-34 was placed in $Cu(CH_3COO)_2$ solution, without calcination and NH_4^+ exchange, and stirred at 50 °C for 4 h. The sample was removed by centrifugation, washed, and dried at 100 °C overnight. Details of the ion-exchange conditions are shown in Table 1. Before the catalytic activity tests, the template was removed by calcination in air at 600 °C for 5 h. The prepared catalysts are denoted by Cu_x-H-Si and Cu_x-L-Si, where *x* represents the Cu loading (wt%).

2.2. Characterization

The elemental compositions of the samples were determined using X-ray fluorescence (XRF) spectroscopy (PANalytical Axios Advanced). N_2 adsorption-desorption isotherms were recorded using a Micromeritics ASAP 2020 instrument at liquid-nitrogen temperature. The samples were degassed at 350 °C for about 240 min under a pressure of 10 μm Hg before

Table 1
Ion-exchange conditions and elemental compositions of samples.

Sample [a]	L/S [b]	Concentration of $Cu(OAc)_2$ (mol/L)	Cu content [c] (wt%)
$Cu_{0.68}$-L-Si	30	0.01	0.68
$Cu_{0.61}$-H-Si	8	0.01	0.61
$Cu_{1.37}$-H-Si	20	0.01	1.37
$Cu_{3.67}$-H-Si	25	0.05	3.67

[a] The elemental compositions of H-Si and L-Si precursors are $Al_{0.46}Si_{0.19}P_{0.35}$ and $Al_{0.5}Si_{0.07}P_{0.43}$, respectively. [b] The liquid (mL)/solid (g) ratio for ion exchange (50 °C, 4 h). [c] The metal content is determined by XRF.

analysis.

Solid-state NMR spectroscopy was performed using a Bruker Avance III 600 instrument equipped with a 14.1 T wide-bore magnet and a 4 mm magic-angle spinning (MAS) probe. The resonance frequency for ^{29}Si was 119.2 MHz. ^{29}Si MAS NMR spectra were recorded at a spinning rate of 8 kHz using high-power proton decoupling. The resonance frequencies for ^{27}Al and ^{31}P were 156.4 and 242.9 MHz, respectively. ^{27}Al MAS NMR spectra were recorded using a one-pulse sequence; 200 scans were accumulated and a $\pi/8$ pulse width of 0.75 μs and a 2 s recycle delay were used. Chemical shifts were referenced to $(NH_4)Al(SO_4)_2{\cdot}12H_2O$ at −0.4 ppm. ^{31}P MAS NMR spectra were recorded using high-power proton decoupling; 32 scans were accumulated and a $\pi/4$ pulse width of 1 μs and a 10 s recycle delay were used. Chemical shifts were referenced to 85% H_3PO_4 at 0 ppm.

NH_3-TPD and N_2O chemisorption were performed using a Micromeritics Auto Chem II instrument. The samples for NH_3-TPD were pretreated with He (20 mL/min) at 650 °C for 1 h, and then cooled to 100 °C. The pretreated samples were saturated with NH_3 (6% in helium, 10 mL/min) for 30 min and then purged with He (30 mL/min) to remove physically adsorbed NH_3. The TPD experiments were performed from 100 to 650 °C at a heating rate of 10 °C/min. The samples for N_2O chemisorption experiments were pretreated with N_2 at 350 °C for 1 h and then cooled to room temperature. Before N_2O chemisorption, the samples were reduced with H_2 at 350 °C; the temperature was kept at 350 °C for 5 min to ensure complete reduction of CuO. After reduction, the sample was cooled to 60 °C for N_2O chemisorption. N_2O (0.3% in N_2, 7 mL/min) was passed through the sample until N_2O consumption stopped. The concentration of N_2O in the fluent was determined using mass spectrometry (Omnistar). H_2-TPR was performed on Micromeritics Auto Chem II. About 0.2 g sample was pretreated at 550 °C for 1 h in Ar and then cooled to 100 °C. The TPR procedure was conducted from 100 to 900 °C at a rate of 10 °C/min under 10% H_2-90% Ar (30 mL/min). The consumption of H_2 was detected by a TCD detector.

EPR spectroscopy was performed using a Bruker A 200 instrument. Before the spectrum was recorded, the sample was degassed under a vacuum of 10 μm Hg at 120 °C for 4 h and then sealed in a quartz tube for characterization. The microwave power was 10 mW and the frequency was 9.31 GHz. The sweep width was 2000 G and the sweep time was 84 s, modulated at 100 kHz with a 3 G amplitude. A time constant of 41 ms was used.

2.3. LTST and catalytic activity testing

For LTST, the calcined Cu-SAPO-34 catalysts (60–80 mesh) were placed in quartz tubes of internal diameter 9.5 mm and exposed to a feed consisting of 10% H_2O balanced with N_2 at 50 °C for 11 h. The total flow rate was 265 mL/min. After steam treatment, the catalyst was dried at 150 °C in air overnight. The steam-treated Cu-SAPO-34 catalysts are denoted by Cu_x-H-Si/H and Cu_x-L-Si/H.

The catalytic activity measurements were performed in a fixed-bed quartz reactor of internal diameter 9.5 mm. The calcined catalyst (60–80 mesh, 0.1 g) was diluted with quartz (60–80 mesh, 0.4 g) and then sealed in a quartz tube with quartz wool. Fourier-transform infrared spectroscopy (Bruker Tensor 27 instrument equipped with a gas cell) was used to determine the concentrations of NO, NO_2, N_2O, and NH_3. Under real working conditions, a high gas hourly space velocity (GHSV) is needed to reduce the volume of the deNO_x section. We therefore controlled the feed gas flow in the experiments at 300 mL/min, which is equivalent to a GHSV of 180000 h^{-1}. Before use in a standard SCR reaction, the catalyst was purged with N_2 at 600 °C for 40 min and cooled to the reaction temperature. A feed gas containing 500 ppm NH_3, 500 ppm NO, 5% H_2O, 5% O_2, and balance N_2 was introduced into the reactor. NO conversion was examined from 120 to 550 °C. The temperature was maintained for at least 30 min at each stage to achieve a steady state.

NH_3 oxidation was performed using a similar procedure, except NO was not included in the feed gas.

3. Results and discussion

3.1. Catalyst characterization

Two SAPO-34 molecular sieve samples, with low and high Si contents (i.e., L-Si and H-Si), were used as catalyst supports. Four Cu-SAPO-34 samples were prepared using our recently reported DIE method [21]. Details of the ion-exchange conditions and Cu loadings on the catalysts are given in Table 1. The Cu loadings on the H-Si samples were 0.61, 1.37, and 3.67 wt%, respectively. The Cu loading on $Cu_{0.68}$-L-Si was similar to that on $Cu_{0.61}$-H-Si.

The N_2 adsorption-desorption isotherms of the samples were used to investigate the structural changes in the Cu-SAPO-34 catalysts caused by LTST; the results are shown in Table 2. The surface areas and micropore volumes of the fresh high-silica samples gradually decreased with increasing Cu loading. This is because of the weak acidity of the ion-exchange solution, and indicates that DIE provides better protection against the negative effects of ion exchange on the SAPO framework compared with the conventional method [21]. LTST significantly reduced the surface area and micropore volume of $Cu_{0.61}$-H-Si, which has a low Cu content. The textural properties

Table 2
Textual properties of catalysts before and after low-temperature steam treatment.

Sample	Surface area (m^2/g)		Pore volume (cm^3/g)	
	S_{BET}	S_{micro}	V_{micro}	V_{total}
$Cu_{0.68}$-L-Si	553.68	531.60	0.26	0.28
$Cu_{0.61}$-H-Si	505.90	484.19	0.24	0.27
$Cu_{1.37}$-H-Si	473.57	447.12	0.22	0.26
$Cu_{3.67}$-H-Si	456.08	430.52	0.21	0.25
$Cu_{0.68}$-L-Si /H*	540.86	521.03	0.26	0.28
$Cu_{0.61}$-H-Si /H*	410.99	387.59	0.20	0.25
$Cu_{1.37}$-H-Si /H*	461.51	438.44	0.22	0.25
$Cu_{3.67}$-H-Si /H*	450.25	427.62	0.21	0.25

*The sample code with /H stands for low temperature steaming treated samples.

of $Cu_{1.37}$-H-Si and $Cu_{3.67}$-H-Si, which have higher Cu contents, were well preserved. These results indicate that the $Cu_{1.37}$-H-Si and $Cu_{3.67}$-H-Si frameworks are more resistant to LTST than $Cu_{0.61}$-H-Si is, indicating that a higher Cu content better protects the SAPO framework. LTST had less effect on the textural properties of the low-silica sample $Cu_{0.68}$-L-Si, showing that it had good low-temperature hydrothermal stability. The difference between the stabilities of $Cu_{0.68}$-L-Si and $Cu_{0.61}$-H-Si (with similar Cu contents) confirms that the high-silica sample, with more free bridging hydroxyl groups, is prone to structural damage in a low-temperature steam environment.

Solid-state ^{29}Si, ^{27}Al, and ^{31}P MAS NMR spectroscopies were used to further evaluate the microstructural change in the samples caused by LTST. The ^{29}Si MAS NMR spectra are shown in Fig. 1 and the corresponding deconvoluted results are listed in Table 3.

The ^{29}Si NMR spectrum of the fresh low-silica sample $Cu_{0.68}$-L-Si had one single-resonance peak at around −95 ppm, in accordance with the presence of only Si(4Al) species in the framework. LTST caused little change in the spectrum except slight peak broadening and the emergence of a weak peak at around −85 ppm, implying that the $Cu_{0.68}$-L-Si sample had good stability. For the fresh high-silica Cu-SAPO-34 samples, complex Si environments were observed, with resonances at −94.6, −99.9, −105, −110, and −115.3 ppm in the ^{29}Si spectra, arising from Si(4Al), Si(3Al), Si(2Al), Si(1Al), and Si islands, respectively [22]. The higher content of Si(4Al) species in fresh $Cu_{0.61}$-H-Si (Table 3) is consistent with its better texture, as shown by N_2 physisorption. LTST caused significant changes in the spectra of all three high-silica samples, with the appearance of a strong resonance at −90.4 ppm, which corresponds to $Si(OAl)_3(OH)$ or $Si(OSi)(OAl)_2(OH)$ species at defect sites [23,24]. This is caused by hydrolysis of Si–O–Al bonds. The highest content of Si defect sites was observed for $Cu_{0.61}$-H-Si/H; this is consistent with its low surface area and pore volume. The amount of Si defect sites decreased with increasing Cu loading to 1.37%, indicating improvement of the low-temperature hydrothermal stability of the sample as a result of protection by the increasing number of Cu ions on the negative Si–O–Al bonds. However, further increasing the ion-exchange level to a Cu loading of 3.67% did not further

Table 3
Deconvoluted results for various Si species based on ^{29}Si MAS NMR spectra of samples.

Sample	Defective site	Si(4Al)	Si(3Al)	Si(2Al)	Si(1Al)	Si(0Al)
$Cu_{0.61}$-H-Si	0.05	0.60	0.09	0.09	0.13	0.05
$Cu_{0.61}$-H-Si /H	0.34	0.21	0.12	0.11	0.14	0.07
$Cu_{1.37}$-H-Si	0.06	0.41	0.13	0.17	0.16	0.07
$Cu_{1.37}$-H-Si /H	0.28	0.22	0.15	0.12	0.15	0.08
$Cu_{3.67}$-H-Si	0.03	0.42	0.12	0.19	0.15	0.09
$Cu_{3.67}$-H-Si/H	0.24	0.24	0.15	0.13	0.14	0.10

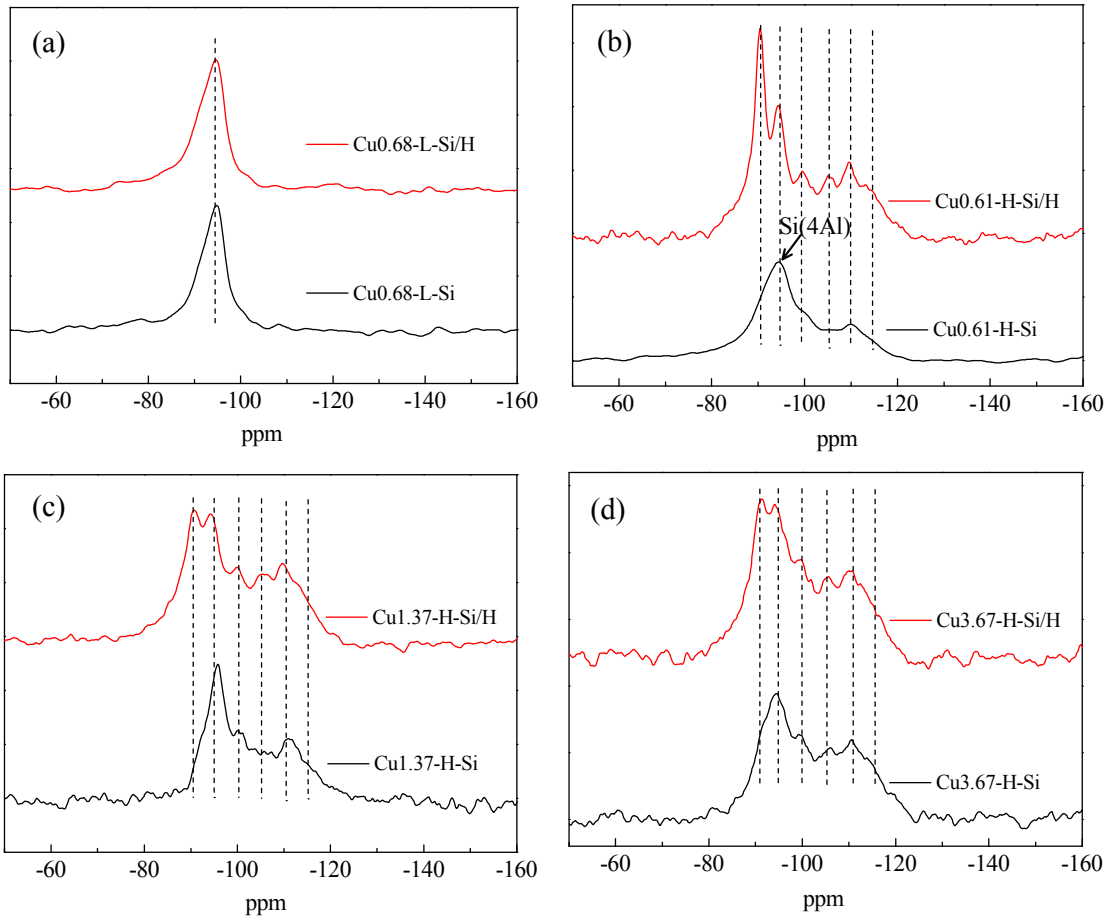

Fig. 1. ^{29}Si MAS NMR spectra of Cu-SAPO-34 samples before and after low-temperature steam treatment.

improve maintenance of the Si environment. This implies that it is not the higher Cu loading, the better structural stability. This is unexpected and is possibly a result of the negative effects of migration and aggregation of Cu species when they are present in large amounts on the CHA support. Evidence of this was obtained using EPR spectroscopy and N_2O chemisorption. The ^{27}Al and ^{31}P spectra of $Cu_{0.68}$-L-Si and $Cu_{0.68}$-H-Si are shown in Fig. 2; both gave one single-resonance peak, in accordance with tetrahedral Al and P(4Al) environments, respectively. The ^{27}Al and ^{31}P spectra of the samples after LTST were little changed. Considering the formation of a large amount of Si defect sites in $Cu_{0.68}$-H-Si/H as a result of hydrolysis of Si–O–Al bonds, the unchanged ^{27}Al spectrum suggests low sensitivity to changes in the tetrahedral Al coordination environments, e.g., from Al(3P)(1Si) to Al(3P)(OH).

The acid properties of the samples were investigated based on NH_3-TPD; the profiles are shown in Fig. 3. The relative amounts of acid in the samples were deconvoluted using Gauss functions; the results are given in Table 4. Clearly, the NH_3-TPD curves could be deconvoluted into three peaks centered at around 175, 300, and 430 °C. The low-temperature (LT) desorption peak corresponds to weakly bound NH_3, and probably consists of contributions from physisorbed NH_3 and NH_3 adsorbed on lattice defects or terminal P(OH) [25] and Al(OH). The medium-temperature (MT) and high-temperature (HT) peaks are attributed to NH_3 desorption from acid sites of moderate and strong strengths, respectively. Both these peaks are related to the NH_4^+ ions formed at Brønsted acid sites (bridging

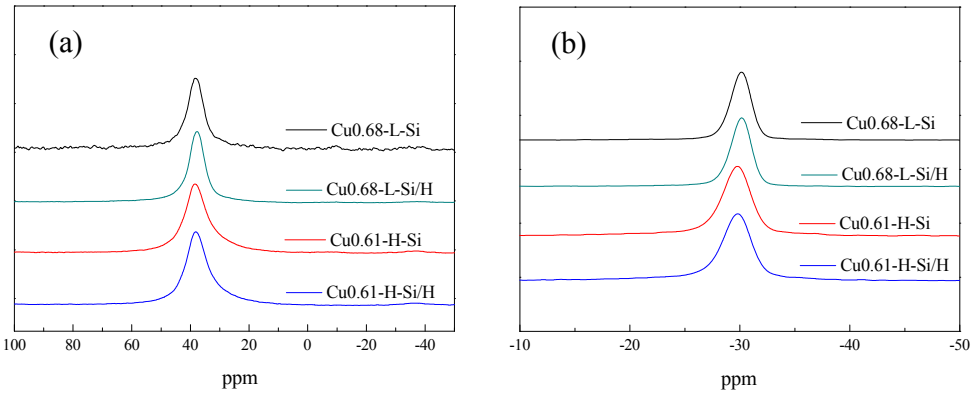

Fig. 2. ^{27}Al (a) and ^{31}P (b) MAS NMR spectra of Cu-SAPO-34 samples before and after low-temperature steam treatment.

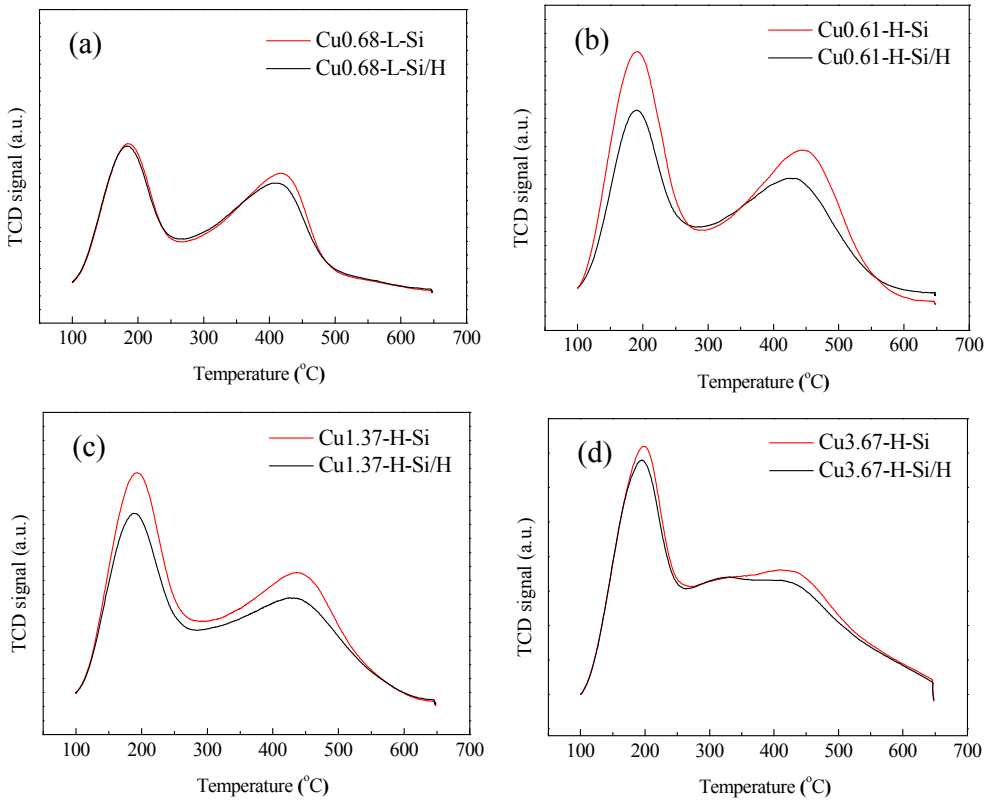

Fig. 3. NH_3-TPD profiles of Cu-SAPO-34 samples before and after low-temperature steam treatment. All figures have the same Y-scale length.

Table 4
Relative acid densities of samples before and after low-temperature steam treatment, determined using NH_3-TPD.

Sample	Before (B)*			Total	After (A)*			Total	A/B
	LT	MT	HT		LT	MT	HT		
$Cu_{0.68}$-L-Si	0.24	0.11	0.23	0.58	0.22	0.13	0.21	0.56	0.97
$Cu_{0.61}$-H-Si	0.42	0.14	0.40	0.95	0.29	0.14	0.31	0.74	0.77
$Cu_{1.37}$-H-Si	0.36	0.17	0.37	0.90	0.28	0.18	0.30	0.76	0.84
$Cu_{3.67}$-H-Si	0.34	0.30	0.36	1.00	0.33	0.31	0.33	0.97	0.97

* The values shown for LT, MT and HT are the relative acid density. $Cu_{3.67}$-H-Si was treated as 1.00.

hydroxyl groups, Si–OH–Al). Moreover, the MT peak intensity clearly increased with increasing Cu content, therefore Lewis acid sites generated by the loaded Cu species also contributed to the moderate acid sites [10].

Among the fresh samples, $Cu_{0.68}$-L-Si had the lowest acid density and lowest acid strength because of its low silica content and the absence of Si islands. It retained 97% of its total acid density after LTST (Table 4), which is in line with its well-preserved framework structure, as shown by the above results. For the fresh samples with high silica contents, the moderate acid density increased at the expense of the strong acid density with increasing Cu loading. This is related to the occupation of strong Brønsted acid sites by the exchanged Cu ions and the generation of Lewis acid sites. $Cu_{0.61}$-H-Si suffered the most serious reduction in acid density as a result of LTST because of the low Cu loading and limited protection of its SAPO framework. The decreases in the acid densities of the Cu-H-Si samples became milder with increasing level of ion exchange; only a 3% decrease in the total amount of acid was observed for $Cu_{3.67}$-H-Si.

It has been reported that isolated Cu^{2+} ions are the active sites in Cu-CHA catalysts for the standard NH_3-SCR reaction [9,10,26,27]. We investigated the location and content of isolated Cu^{2+} ions using EPR spectroscopy, which is only responsive to isolated Cu^{2+} ions [15] and can provide quantitative results. As shown in Fig. 4, the Cu^{2+} species on all the samples had the same coordination environments, with $g_{//}$ values of 2.394 and $A_{//}$ values of 0.110, irrespective of the Cu content and moisture treatment. According to the literature, the EPR signals correspond to isolated Cu ions located at site (I) of the CHA cage [27,28], which coordinate with three oxygen atoms of the six-membered rings. Such a location is expected to facilitate contact between Cu ions and reactants such as NO [27].

Table 5 lists the Cu^{2+} contents of the samples. For the

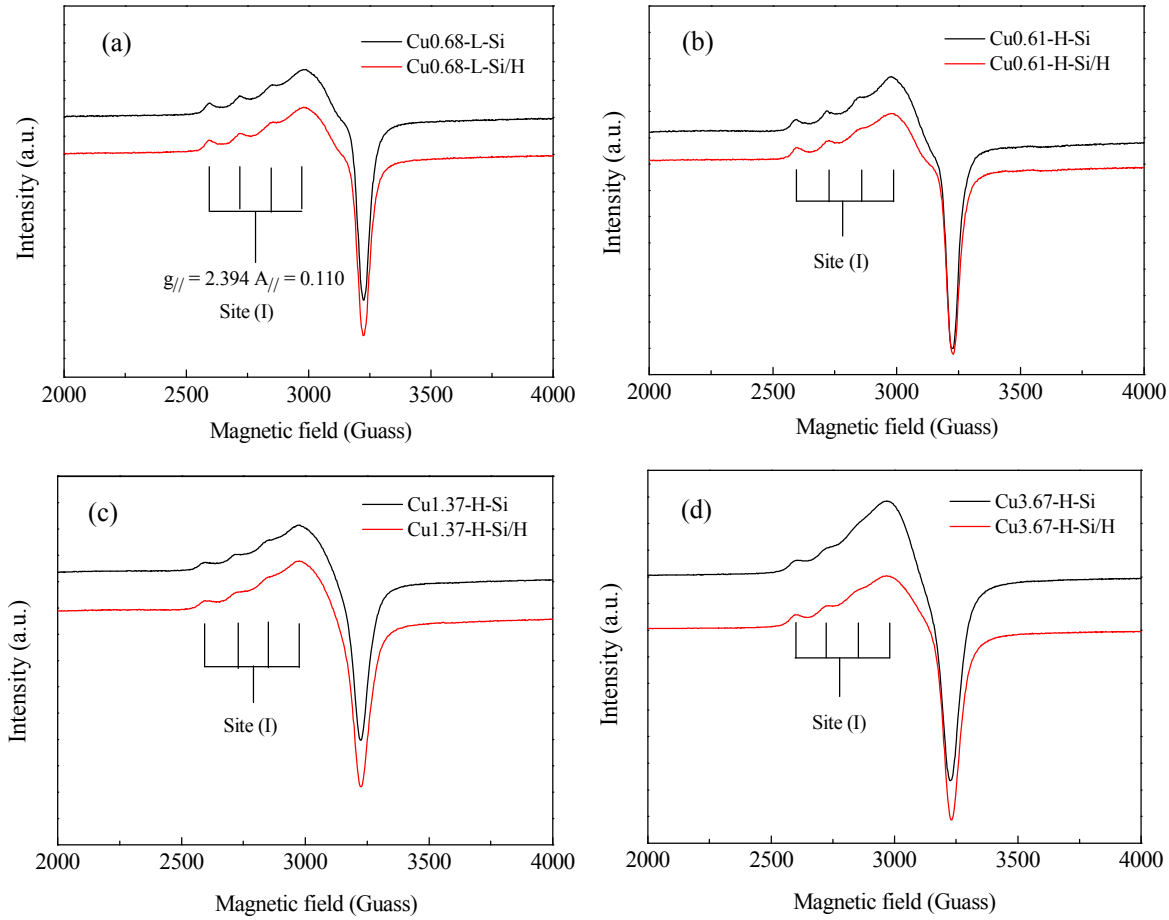

Fig. 4. EPR spectra of samples before and after low-temperature steam treatment.

Table 5
Isolated Cu^{2+} contents of samples before and after low-temperature steam treatment, determined using EPR spectroscopy.

Sample	Before *	After *	After/Before
$Cu_{0.68}$-L-Si	0.294	0.292	0.993
$Cu_{0.61}$-H-Si	0.292	0.264	0.904
$Cu_{1.37}$-H-Si	0.525	0.535	1.019
$Cu_{3.67}$-H-Si	1.000	0.781	0.781

* The isolated Cu^{2+} content on $Cu_{3.67}$-H-Si is defined as 1.000.

low-silica sample $Cu_{0.68}$-L-Si, the amount of isolated Cu^{2+} was almost unchanged after LTST, in accordance with its well-preserved framework structure. For the fresh high-silica samples, the isolated Cu^{2+} contents gradually increased with increasing Cu loading. LTST decreased the amount of Cu^{2+} in $Cu_{0.61}$-H-Si by 10%. Its Brunauer-Emmett-Teller (BET) surface area decreased by 20%, suggesting that framework deterioration results in the loss of a small amount of Cu^{2+} ions. $Cu_{1.37}$-H-Si suffered less structural damage than $Cu_{0.61}$-H-Si and therefore retained its Cu^{2+} content well; the increased framework stability led to better retention of Cu^{2+}. However, $Cu_{3.67}$-H-Si lost about 22% of its Cu^{2+} ions, which is a bigger drop than in the cases of $Cu_{0.61}$-H-Si and $Cu_{1.37}$-H-Si, with lower Cu contents. This could be because adsorbates such as H_2O cause movement of Cu^{2+} out of site (I) on samples with high Cu contents [29]. The Cu^{2+} ions in new locations are not as stable as those located at site (I) [30], and tend to migrate/aggregate, causing a decrease in the number of isolated Cu ions. These results show that the stability of the Cu ions and that of the SAPO framework are positively correlated at low Cu loadings, but a high Cu loading (e.g., 3.67 wt%) would decrease the number of isolated Cu ions during LTST.

3.2. *NH_3 oxidation reaction and N_2O chemisorption*

NH_3 oxidation is the main side reaction in NH_3-SCR. It consumes NH_3 in the standard NH_3-SCR reaction, leading to a drop in NO conversion. NH_3 oxidation is generally negligible at low temperatures, but becomes more severe with increasing reaction temperature. The NH_3 oxidation reaction is closely related to the amount of CuO [31,22] and the acid properties [32] of the catalyst. The O_2 concentration can affect the activation and oxidation of NH_3 molecules [33]. A sample with a higher Cu loading is generally more active in NH_3 oxidation [34] because the amount and percentage of CuO can both increase with increasing Cu content. However, an increase in the acid density inhibits NH_3 oxidation [32], facilitating NH_3-SCR. The NH_3 oxidation results for the samples are shown in Fig. 5. For the fresh samples, the order of the oxidation activity was $Cu_{3.67}$-H-Si > $Cu_{0.68}$-L-Si > $Cu_{1.37}$-H-Si > $Cu_{0.61}$-H-Si. This sequence is reasonable because $Cu_{3.67}$-H-Si has the highest Cu content, probably resulting in a large amount of CuO, which contributes to the NH_3 oxidation activity; $Cu_{0.61}$-H-Si, with a low Cu content, has less CuO and more acid sites, which could suppress NH_3 oxidation and lead to low NH_3 conversion.

The NH_3 conversions over $Cu_{3.67}$-H-Si and $Cu_{0.68}$-L-Si after LTST declined, but less change was observed in the cases of

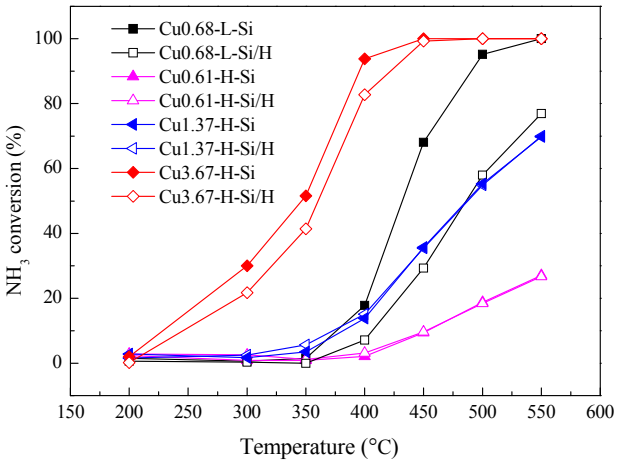

Fig. 5. NH_3 oxidation reaction over samples before and after low-temperature steam treatment. Reaction condition: feed gas consisted of 500 ppm NH_3, 5% O_2, 5% H_2O, balance N_2; GHSV = 180000 h^{-1}.

$Cu_{1.37}$-H-Si and $Cu_{0.61}$-H-Si. These results are unexpected because all the samples showed a decrease in the total amount of acid and/or isolated Cu^{2+} content (corresponding to the generation of more CuO), which should result in an increase in NH_3 conversion. We suggest that some of the CuO particles on Cu-SAPO-34 aggregate during LTST (verified later), which leads to a reduction in the surface area of CuO particles and therefore a decline in the NH_3 oxidation activity. The observed decreased or nearly unchanged NH_3 oxidation activity is therefore a result of the balance of three factors: (1) the decreased acid amount (positive); (2) the partial loss of Cu^{2+} that can be converted to CuO (positive); and (3) the aggregation of CuO particles (negative).

We performed N_2O chemisorption experiments over fresh and treated $Cu_{3.67}$-H-Si to determine whether partial aggregation of CuO particles occurred. N_2O chemisorption is a classical method for determining Cu dispersion [35], and has been widely studied [36–40]; it is considered to be more accurate than CO adsorption [41] and H_2-TPD [42] for determining the surface area of Cu atoms. N_2O reacts with Cu atoms stoichiometrically according to the following equation:

$$N_2O + 2Cu \rightarrow N_2 + (Cu–O–Cu)$$

In principle, the Cu atoms on the external surface react with N_2O at low temperatures and the bulk Cu atoms can only react with N_2O at high temperatures.

We estimated the surface area of CuO particles by measuring the surface area of Cu atoms on the partially reduced catalysts. H_2-TPR was conducted to determine the reduction temperatures for $Cu_{3.67}$-H-Si and $Cu_{3.67}$-H-Si/H before N_2O chemisorption. The H_2-TPR results are shown in Fig. 6; the curves show two reduction peaks centered at around 190 and 600 °C.

The lower-temperature peak is attributed to the complete reduction of CuO (possibly including partial reduction of Cu^{2+} to Cu^+) and the higher-temperature peak probably arises from further reduction of Cu ions to Cu [10]. The sample was reduced at 350 °C with H_2 (6% in Ar) and then N_2O chemisorption was performed at 60 °C. We used reactive frontal chromatography to perform the experiments and mass spectrometry was used to determine the N_2O concentration at the outlet. The

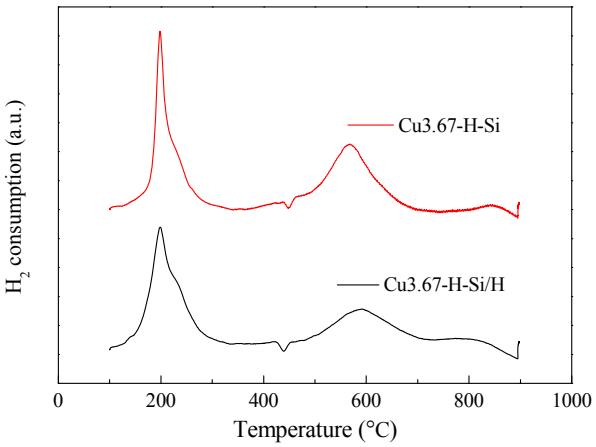

Fig. 6. H_2-TPR results for $Cu_{3.67}$-H-Si and $Cu_{3.67}$-H-Si/H.

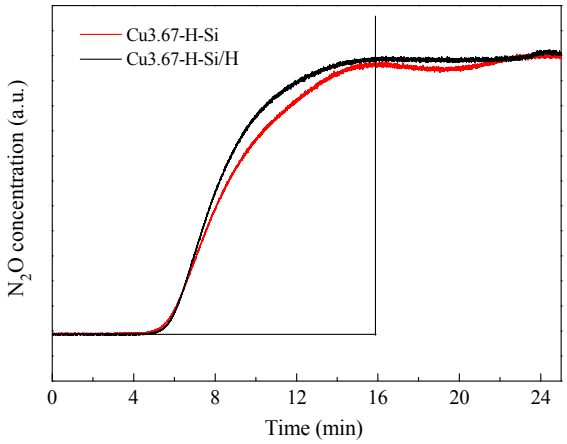

Fig. 7. N_2O chemisorption on $Cu_{3.67}$-H-Si and $Cu_{3.67}$-H-Si/H at 60 °C. Samples were reduced at 350 °C before N_2O chemisorption. N_2O concentration was determined using mass spectrometry.

results are shown in Fig. 7. The area between the profile and baseline is the amount of N_2O that remained at the outlet. The N_2O consumption by $Cu_{3.67}$-H-Si/H was about 94% of that by $Cu_{3.67}$-H-Si, suggesting a larger Cu (CuO) surface area and smaller CuO particles on the fresh sample. Given that $Cu_{3.67}$-H-Si lost 22% of its Cu^{2+}, which can form CuO during LTST, the aggregation of CuO particles becomes a more convincing hypothesis.

3.3. *NH_3-SCR performance*

The results for standard NH_3-SCR reactions over the samples are shown in Fig. 8. Of the fresh samples, the low-silica sample $Cu_{0.68}$-L-Si showed the worst SCR activity because of its low Cu loading and low acid density. The NO conversion over the three high-silica samples increased with increasing Cu loading, especially in the low-temperature range, i.e., less than 300 °C.

LTST deactivated all the samples. $Cu_{1.37}$-H-Si showed the least deactivation (mainly in the low-temperature range), whereas $Cu_{3.67}$-H-Si showed significant deactivation in both the low- and high-temperature ranges. $Cu_{0.68}$-L-Si and $Cu_{0.61}$-H-Si showed similar declines in activation.

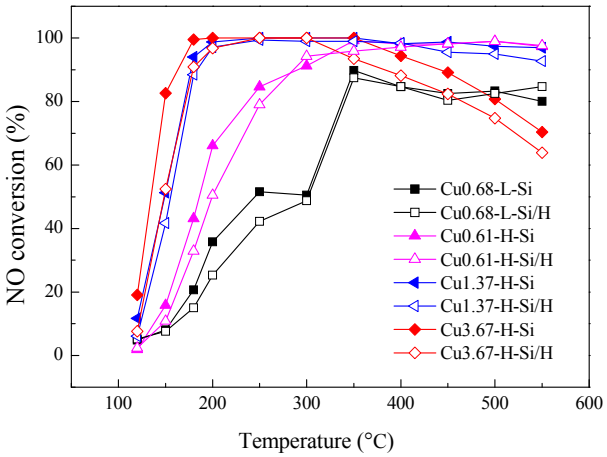

Fig. 8. Standard SCR reaction over samples before and after low-temperature steam treatment. Reaction conditions: feed gas consisted of 500 ppm NH_3, 500 ppm NO, 5% H_2O, 5% H_2O, balance N_2; GHSV = 180000 h^{-1}.

NO_x is mainly desorbed from Cu-based zeolites at temperatures higher than 200 °C [15,43]. It has been suggested that NH_3-SCR follows a Langmuir-Hinshelwood mechanism at low temperatures [25], in which the adsorbed NH_3 reacts with the nitrite or nitrate species formed over active Cu species to generate key intermediates, i.e., the acid properties and isolated Cu ions both play important roles in the reaction [25,44]. The slight difference between the low-temperature deactivations of the low-Cu samples $Cu_{0.68}$-L-Si and $Cu_{0.61}$-H-Si is interesting because the acid density, structural integrity, and number of Cu ions of the latter decreased more than those of the former as a result of LTST. It is supposed that the remaining acid density of $Cu_{0.61}$-H-Si/H was sufficiently high, and excessive relative to its low Cu^{2+} content, which helps the sample showing less reduced NO conversion [32]. $Cu_{1.37}$-H-Si retained its Cu^{2+} content well, sustained only slight structural damage, and showed a 16% decrease in acid density after LTST. The amount of acid on $Cu_{1.37}$-H-Si/H could still be sufficient for Cu^{2+} ions, leading to better preservation of the NH_3-SCR activity. The deactivation of $Cu_{3.67}$-H-Si by LTST was the most severe among all the samples, although $Cu_{3.67}$-H-Si/H still showed good low-temperature SCR activity. The low-temperature deactivation was mainly caused by loss of Cu^{2+} ions (22% drop) from the sample. $Cu_{3.67}$-H-Si/H was the only sample that showed serious high-temperature deactivation compared with the fresh precursor. The slightly reduced NH_3 oxidation activity of $Cu_{3.67}$-H-Si/H described above is favorable for high-temperature NH_3-SCR, therefore the high-temperature activity decline is again attributed to loss of active Cu^{2+} ions.

4. Conclusions

Cu-SAPO-34 catalysts with various Si contents and Cu loadings were prepared, and their low-temperature hydrothermal stabilities were investigated. The results show that incorporation of Cu ions improves the stability of the SAPO-34 framework and its textural properties and acidity. At the same Cu loading, Cu-SAPO-34 with more bridging hydroxyl groups (a higher Si content) is more prone to framework degradation on

exposure to low-temperature moisture. The stabilities of isolated Cu^{2+} ions and the SAPO framework are closely related but different. When the ion-exchange level is low, the stability of the Cu^{2+} ions is positively correlated with that of the Cu^{2+}-protected framework. However, when the ion-exchange level is relatively high (e.g., 3.67 wt% Cu loading), some of the Cu^{2+} ions migrate out of sites (I) as a result of LTST, and lose their stability; this decreases the isolated Cu^{2+} content. The CuO particles on Cu-SAPO-34 are also unstable and aggregate during LTST, which accounts for the observed decrease in the NH_3 oxidation activities of the catalysts. All the treated Cu-SAPO-34 catalysts showed decreased NH_3-SCR activity (mainly in the low-temperature range) as a result of loss of isolated Cu^{2+} and/or acid sites. The NH_3-SCR activity of high-Si Cu-SAPO-34 with a 1.37 wt% Cu loading was better preserved because of its well-retained Cu^{2+} content and lower reduction in acid density.

References

[1] K. Skalska, J. S. Miller, S. Ledakowicz, *Sci. Total Environ.,* **2010**, 408, 3976–3989.
[2] F. D. Liu, Y. B. Yu, H. He, *Chem. Commun.,* **2014**, 50, 8445–8463.
[3] M. Koebel, M. Elsener, M. Kleemann, *Catal. Today,* **2000**, 59, 335–345.
[4] Z. X. Ma, H. S. Yang, F. Liu, X. B. Zhang, *Appl. Catal. A,* **2013**, 467, 450–455.
[5] J. P. Chen, R. T. Yang, *Appl. Catal. A,* **1992**, 80, 135–148.
[6] E. T. C. Vogt, A. van Dillen, J. W. Geus, F. J. J. G. Janssen, *Catal. Today,* **1988**, 2, 569–579.
[7] B. M. Abu–Zied, W. Schwieger, A. Unger, *Appl. Catal. B,* **2008**, 84, 277–288.
[8] H. Sjövall, E. Fridell, R. J. Blint, L. Olsson, *Top. Catal.,* **2007**, 42–43, 113–117.
[9] L. Wang, W. Li, G. S. Qi, D. Weng, *J. Catal.,* **2012**, 289, 21–29.
[10] D. Wang, L. Zhang, J. H. Li, K. Kamasamudram, W.S. Epling, *Catal. Today,* **2014**, 231, 64–74.
[11] D. W. Fickel, E. D'Addio, J. A. Lauterbach, R. F. Lobo, *Appl. Catal. B,* **2011**, 102, 441–448.
[12] I. Lezcano-Gonzalez, U. Deka, B. Arstad, A. Van Yperen-De Deyne, K. Hemelsoet, M. Waroquier, V. Van Speybroeck, B. M. Weckhuysen, A. M. Beale, *Phys. Chem. Chem. Phys.,* **2014**, 16, 1639–1650.
[13] F. Gao, E. D. Walter, M. Kollar, Y. L. Wang, J. Szanyi, C. H. F. Peden, *J. Catal.,* **2014**, 319, 1–14.
[14] E. Borfecchia, K. A. Lomachenko, F. Giordanino, H. Falsig, P. Beato, A. V. Soldatov, S. Bordiga, C. Lamberti, *Chem. Sci.,* **2015**, 6, 548–563.
[15] L. Ma, Y. S. Cheng, G. Cavataio, R. W. McCabe, L. X. Fu, J. H. Li, *Chem. Eng. J.,* **2013**, 225, 323–330.
[16] M. Briend, R. Vomscheid, M. J. Peltre, P. P. Man, D. Barthomeuf, *J. Phys. Chem.,* **1995**, 99, 8270–8276.
[17] F. D. P. Mees, L. R. M. Martens, M. J. G. Janssen, A. A. Verberckmoes, E. F. Vansant, *Chem. Commun.,* **2003**, 44–45.
[18] Z. B. Li, J. Martinez-Triguero, P. Concepcion, J. H. Yu, A. Corma, *Phys. Chem. Chem. Phys.,* **2013**, 15, 14670–14680.
[19] J. Wang, D. Q. Fan, T. Yu, J. Q. Wang, T. Hao, X. Q. Hu, M. Q. Shen, W. Li, *J. Catal.,* **2015**, 322, 84–90.
[20] K. Leistner, L. Olsson, *Appl. Catal. B,* **2015**, 165, 192–199.
[21] X. Xiang, M. Yang, B. B. Gao, Y. Y. Qiao, P. Tian, S. T. Xu, Z. M. Liu, *RSC Adv.,* **2016**, 6, 12544–12552.
[22] T. Yu, D. Q. Fan, T. Hao, J. Wang, M. Q. Shen, W. Li, *Chem. Eng. J.,* **2014**, 243, 159–168.
[23] N. Katada, K. Nouno, J. K. Lee, J. Shin, S. B. Hong, M. Niwa, *J. Phys. Chem. C,* **2011**, 115, 22505–22513.
[24] K. Suzuki, T. Nishio, N. Katada, G. Sastre, M. Niwa, *Phys. Chem. Chem. Phys.,* **2011**, 13, 3311–3318.
[25] D. Wang, L. Zhang, K. Kamasamudram, W. S. Epling, *ACS Catal.,* **2013**, 3, 871–881.
[26] U. Deka, I. Lezcano-Gonzalez, S. J. Warrender, A. Lorena Picone, P. A. Wright, B. M. Weckhuysen, A. M. Beale, *Microporous Mesoporous Mater.,* **2013**, 166, 144–152.
[27] J. J. Xue, X. Q. Wang, G. S. Qi, J. Wang, M. Q. Shen, W. Li, *J. Catal.,* **2013**, 297, 56–64.
[28] J. Wang, T. Yu, X. Q. Wang, G. S. Qi, J. J. Xue, M. Q. Shen, W. Li, *Appl. Catal. B,* **2012**, 127, 137–147.
[29] J. Szanyi, J. H. Kwak, H. Zhu, C. H. F. Peden, *Phys. Chem. Chem. Phys.,* **2013**, 15, 2368–2380.
[30] Y. J. Kim, J. K. Lee, K. M. Min, S. B. Hong, I. S. Nam, B. K. Cho, *J. Catal.,* **2014**, 311, 447–457.
[31] G. Busca, L. Lietti, G. Ramis, F. Berti, *Appl. Catal. B,* **1998**, 18, 1–36.
[32] T. Yu, J. Wang, M. Shen, W. Li, *Catal. Sci. Technol.,* **2013**, 3, 3234–3241.
[33] B. Li, Z. Y. Ren, Z. X. Ma, X. D. Huang, F. Liu, X. B. Zhang, H. S. Yang, *Catal. Sci. Technol.,* **2016**, 6, 1719–1725.

Graphical Abstract

Chin. J. Catal., 2017, 38: 918–927 doi: 10.1016/S1872-2067(17)62836-5

Investigation of low-temperature hydrothermal stability of Cu-SAPO-34 for selective catalytic reduction of NO_x with NH_3

Xiao Xiang, Pengfei Wu, Yi Cao, Lei Cao, Quanyi Wang, Shutao Xu, Peng Tian *, Zhongmin Liu *
Dalian Institute of Chemical Physics, Chinese Academy of Sciences; University of Chinese Academy of Sciences

The factors that affect the low-temperature hydrothermal stability and NH_3-selective catalytic reduction performances of Cu-SPAO-34 were investigated. An understanding of these factors is important in practical applications.

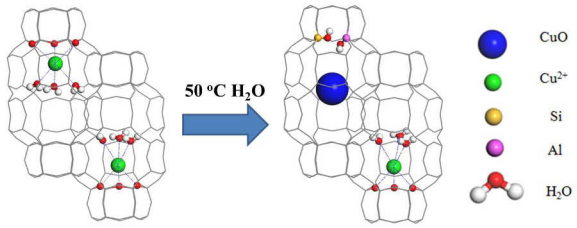

[34] O. Mihai, C. R. Widyastuti, S. Andonova, K. Kamasamudram, J. H. Li, S. Y. Joshi, N. W. Currier, A. Yezerets, L. Olsson, *J. Catal.,* **2014**, 311, 170–181.
[35] L. Q. Ma, Y. C. Fu, J. Y. Shen, *Chin. J. Catal.,* **2003**, 24, 312–316.
[36] J. W. Evans, M. S. Wainwright, A. J. Bridgewater, D. J. Young, *Appl. Catal.,* **1983**, 7, 75–83.
[37] T. J. Osinga, B. G. Linsen, W. P. VanBeek, *J. Catal.,* **1967**, 7, 277–279.
[38] E. Giamello, B. Fubini, P. Lauro, A. Bossi, *J. Catal.,* **1984**, 87, 443–451.
[39] B. Dvorak, J. Pasek, *J. Catal.,* **1970**, 18, 108.
[40] G. C. Chinchen, C. M. Hay, H. D. Vandervell, K. C. Waugh, *J. Catal.,* **1987**, 103, 79–86.
[41] P. H. Emmett, N. Skau, *J. Am. Chem. Soc.,* **1943**, 65, 1029–1035.
[42] M. Muhler, L. P. Nielsen, E. Tornqvist, B. S. Clausen, H. Topsoe, *Catal. Lett.*, **1992**, 14, 241–249.
[43] L. Zhang, D. Wang, Y. Liu, K. Kamasamudram, J. H. Li, W. Epling, *Appl. Catal. B,* **2014**, 156–157, 371–377.
[44] D. S. Zhou, B. Li, Z. X. Ma, X. D. Huang, X. B. Zhang, H. S. Yang, *J. Mol. Catal. A,* **2015**, 409, 183–190.